Magnomechanical phonon laser beyond the steady state

Saeid Vashahri-Ghamsari [1,*] Qing Lin [2] Bing He,[3,†] and Min Xiao[1]

[1]*Department of Physics, University of Arkansas, Fayetteville, Arkansas 72701, USA*
[2]*Fujian Key Laboratory of Light Propagation and Transformation, College of Information Science and Engineering,*
Huaqiao University, Xiamen 361021, China
[3]*Center for Quantum Optics and Quantum Information, Universidad Mayor, Camino La Pirámide 5750, Huechuraba, Chile*

Phonon lasers, the mechanical analogs of optical lasers, have long been a subject of interest as they provide coherent sound waves. We numerically study a magnomechanical phonon laser that operates under a general continuous-wave pump. This system consists of a microwave cavity, a sphere of magnetic material (yttrium iron garnet), a microwave drive pump, and a uniform external bias magnetic field. A population inversion between the supermodes of the system leads to phonon laser action. We study the population inversion and the stimulated emission of phonons under various conditions, such as different drive pump powers and detunings. Unlike previous studies, our results show that the population inversion between the supermodes oscillates with time. Despite the oscillations of the population inversion, one can achieve relatively large stimulated phonon emission if the power of the drive pump is beyond a threshold. Moreover, the optimum operation occurs if the frequency of the drive field matches the frequencies of the cavity photons and magnons. Since it is highly tunable with low loss and has an extra degree of freedom provided by the constant magnetic field, it is possible to develop the system into an alternative to the optomechanical phonon lasers.

I. INTRODUCTION

Phonon lasers generate intensified, coherent sound oscillations (mechanical vibrations) induced by optical pumping [1]. Since sound waves propagate 5 orders of magnitude slower than the speed of light, their wavelength is much shorter than that of light waves of the same frequency [2]. Therefore, one can perform precise, nondestructive measurements and achieve a high concentration of energy using focused sound waves. The phonon laser has potential applications in audio filtering, acoustic imaging, highly precise sensing, imaging or switching, and topological sound control [3–11].

Phonon lasers have been investigated in some platforms such as in a trapped ion system driven by optical forces [12], quantum dots [13–15], superlattices [16], electromechanical resonators [17], and optomechanical systems [1,18–22]. Recently, a phonon laser in a cavity magnomechanical system has been proposed [23,24]. The system includes a microwave cavity, a small sphere of magnetic material, a uniform external bias magnetic field, and a microwave drive pump (Fig. 1). The magnetic material should have a high spin density and a strong spin-spin exchange interaction so that it can support a Kittel mode (uniform magnetostatic mode) [25] with a relatively low damping rate. One of the most promising materials for the magnetic sphere is yttrium iron garnet (YIG), which can have

a strong coupling to cavity photons [26–30], phonons [31], and superconducting qubits [32,33].

Compared with its optomechanical counterpart, the magnomechanical phonon laser introduced in Refs. [23,24] has an additional degree of freedom—an adjustable, uniform magnetic field. Its high tunability enables the cavity magnomechanical systems to be a promising platform to develop various novel phenomena such as microwave-to-optical quantum transducers for quantum information processing [34] and quantum-enhanced detection of magnons in magnon spintronics [35,36]. However, the previous schemes of magnomechanical phonon laser were studied under the assumption of a steady-state condition. As we know from certain optomechanical phonon lasers, say, the $\mathcal{PT}$-symmetric ones, a truly steady state does not exist under the normal operation conditions, and the key parameters, such as the population inversion between the supermodes and the phonon emission, can vary with time [22,37]. In magnomechanical systems, the magnetostriction force (the expansion or contraction of a magnetic material in response to a magnetic field [38]) plays a role similar to the radiation pressure force in optomechanical systems. Therefore, one may ask whether the dynamical behavior of a magnomechanical phonon laser demonstrates is important to its operation. In this paper, we address this question by investigating the magnomechanical phonon laser in the dynamical regime.

We organize the rest of the paper as follows. In Sec. II, we first introduce the system and its Hamiltonian, and then we linearize the nonlinear equations of motion of the system by a special method of decomposing the total time evolution operator [39–41]. Afterward, based on the physical picture in
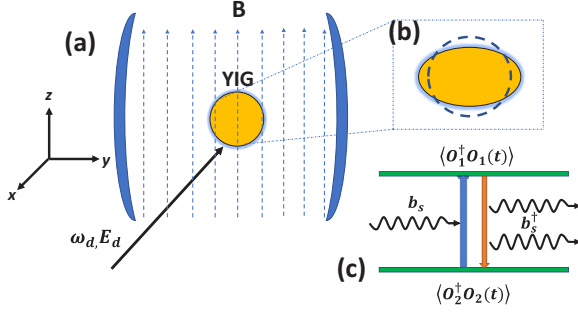
*svashahr@uark.edu
†bing.he@umayor.cl

FIG. 1. Schematic diagram of the magnomechanical phonon laser. Panel (a) shows the magnetic sphere is inserted in the microwave cavity mode. An external magnetic field **B** along the z direction provides a uniform magnon mode for the magnetic sphere. Moreover, we have applied a drive microwave pump with the amplitude E_d and the angular frequency ω_d along the x direction. Panel (b) symbolically shows that the magnetic sphere deforms in response to the magnetic field of the microwave cavity mode. Panel (c) demonstrates the schematic analogy between an optical laser and the phonon laser. Here the stimulated transition of phonons occurs between the two supermode states of the cavity, $\hat{o}_1^\dagger|0\rangle$ and $\hat{o}_2^\dagger|0\rangle$, and their occupation numbers $\langle\hat{o}_i^\dagger\hat{o}_i\rangle$ ($i = 1$ and 2) are generally time dependent in the dynamical operation of the setup.

Sec. III, we simulate the behaviors of the population inversion and the phonon number by considering different parameters in Sec. IV. Finally, in Sec. V, we summarize our results.

II. MODEL AND METHOD

A. System Hamiltonian

Figure 1 shows the scheme of the magnomechanical phonon laser. Like in Ref. [23], we place a highly polished magnetic sphere (regarded as an ensemble of N spins) of 1 mm in diameter in a microwave cavity. Simultaneously, we apply a uniform external bias magnetic field **B** in the vertical direction z. This adjustable magnetic field (varying between 0 and 1 T) collectively excites the spins of the magnetic sample and aligns them along the z direction—magnons. When the static magnetic field is uniform, one calls the corresponding mode the Kittel mode. The magnon mode Hamiltonian is $\hat{H}_{\text{magnon}} = \omega_m \hat{m}^\dagger \hat{m}$, where ω_m is the angular frequency of the magnon mode, and $\hat{m}^\dagger$ and $\hat{m}$ are the creation and annihilation operators of the magnon, respectively. The frequency of the magnon mode is related to the magnetic field by $\omega_m = \gamma_g \mathbf{B}/\mu_0$, where $\gamma_g = 2\pi \times 28$ GHz/T is the gyromagnetic ratio and $\mu_0 = 4\pi \times 10^{-7}$ H/m is the vacuum permeability. The uniform magnetic field establishes the Kittel mode and mediates the coupling between the magnons and cavity photons of the angular frequency ω_a. One can write the Hamiltonian of the cavity photons as $\hat{H}_{\text{photon}} = \omega_a \hat{a}^\dagger \hat{a}$, where $\hat{a}^\dagger$ and $\hat{a}$ are the creation and annihilation operators of the microwave photon in the mode, respectively. The coupling depends on the position of the magnetic sample and the intensity of the magnetic field.

Moreover, we apply a microwave drive pump along the x direction to harmonically excite the magnon mode. Since the directions of **B**, the magnetic field of the drive pump, and

the magnetic field of the cavity mode are perpendicular to each other, we can adjust each one independently. Furthermore, we assume that the diameter of the magnetic sphere is much smaller than the wavelength of the cavity modes so that the photon-photon coupling is negligible. We set the position of the magnetic sphere to the maximum amplitude of the microwave field. The time-dependent magnetic field of the pump harmonically drives the magnons and changes the magnetization. Therefore, the magnetic sphere is harmonically deformed (magnetostriction effect), converting it to a mechanical resonator with the phonon mode of angular frequency ω_b. Thereby, the magnetostrictive interaction leads to the coupling between magnons and phonons. The overlap between the uniform magnon mode and the phonon mode determines the magnetostrictive coupling strength.

The Hamiltonian of the microwave drive pump is $\hat{H}_d = iE_d(\hat{m}^\dagger e^{-i\omega_d t} - \hat{m}e^{i\omega_d t})$, where ω_d is the drive pump frequency and $E_d = \frac{\sqrt{5}}{4}\gamma_g\sqrt{\rho V}\mathcal{B}_0$ is the amplitude of the drive field. In this equation, V is the volume of the magnetic sample, $\rho = 4.22 \times 10^{27}$ m^{-3} is the spin density of the magnetic sphere, and $\mathcal{B}_0$ is the amplitude of the magnetic field of the drive pump [42]. Notice we use the magnetic field of the pump to drive the system and, hence, it includes $\hat{m}$.

The Hamiltonian $\hat{H}_{\text{dipole}} = J(\hat{a}\hat{m}^\dagger + \hat{a}^\dagger\hat{m})$ describes the magnon-photon coupling, which is similar to a scattering of the magnons into the cavity photons through magnetic dipole interaction. The coupling strength J between the Kittel mode and the microwave cavity field mode, which can be tuned by changing the position of the magnetic sphere [23], is given by $\frac{1}{2}g^*\mu_B\delta\mathcal{B}\sqrt{N}$, where g^* is the g factor and μ_B is the Bohr magneton. This coupling is enhanced collectively by the factor $\sqrt{N}$ if there are N fully polarized spins in the unit volume of the ensemble, an effect like the collective enhancement of the atom-field coupling in atomic ensembles. Using an embedded Jaynes-Cummings model, the enhancement by $\sqrt{N}$ times was found for the magnetic dipole coupling of an ensemble of spins to a superconducting microwave stripline structure [43]. The parameter $\delta\mathcal{B}$ is the amplitude of the vacuum fluctuations of the microwave cavity magnetic field in the ferromagnetic crystal, and it is transverse to the external magnetic field. If the microwave magnetic field is uniform throughout the ferromagnetic crystal, the magnetic dipole coupling vanishes except for the uniform magnetostatic (Kittel) mode [34] so that the coupling between higher-order magnetostatic modes and a microwave cavity mode requires a nonuniform cavity magnetic field. If $J \gg \gamma_m, \gamma_a$, where γ_m and γ_a are the damping rates of the magnon and photon modes, the hybrid system will enter the strong coupling regime [36].

The Hamiltonian of the magnomechanical interaction is given by $\hat{H}_M = -g\hat{m}^\dagger\hat{m}(\hat{b} + \hat{b}^\dagger)$, where g is the magnomechanical coupling factor (the derivation of the Hamiltonian is given in the Supplemental Material for Ref. [31]). This interaction is usually negligible in the typical experiments, but one can significantly enhance it by driving the magnon mode with a sufficiently intense microwave field [42].

The total Hamiltonian can be written as the sum of the linear and nonlinear parts:

$$\hat{H} = \hat{H}_{\text{L}} + \hat{H}_{\text{NL}}, \qquad (1)$$

where

$$
\begin{aligned}
\hat{H}_{\mathrm{L}} &= \omega_a \hat{a}^\dagger \hat{a} + \omega_m \hat{m}^\dagger \hat{m} + \omega_b \hat{b}^\dagger \hat{b} + J(\hat{a}^\dagger \hat{m} + \hat{m}^\dagger \hat{a}) \\
&\quad + i E_d (\hat{m}^\dagger e^{-i\omega_d t} - \hat{m}\, e^{i\omega_d t}), \\
\hat{H}_{\mathrm{NL}} &= -g\hat{m}^\dagger \hat{m}(\hat{b} + \hat{b}^\dagger).
\end{aligned} \tag{2}
$$

Then we obtain the differential equations that describe the time evolution of the system operators:

$$
\begin{aligned}
\dot{\hat{a}} &= -(i\omega_a + \gamma_a)\hat{a} - iJ\hat{m}, \\
\dot{\hat{m}} &= -(i\omega_m + \gamma_m)\hat{m} - iJ\hat{a} + ig\hat{m}(\hat{b} + \hat{b}^\dagger) + E_d e^{-i\omega_d t}, \\
\dot{\hat{b}} &= -(\gamma_b + i\omega_b)\hat{b} + ig\hat{m}^\dagger \hat{m},
\end{aligned} \tag{3}
$$

where γ_b is the damping rate of the phonon mode. In our analysis, we apply a strong pumping field so that $|\hat{m}| \gg 1$ and $|\hat{a}| \gg 1$. Moreover, we are primarily concerned with the "coherent" emission of phonons (similar to the coherent emission of photons in an optical laser [44]) instead of the quantum features of the mechanical field (such as the correlations in the mechanical field). Therefore, we neglect the quantum noise contributions in Eq. (3), though they may slightly modify the results without giving a qualitative change as in the coupled cavity systems [45].

The common method to solve the similar systems of nonlinearity is converting each operator (say, $\hat{a}$) to a classical average value plus a quantum fluctuation: $\hat{a} \rightarrow \langle \hat{a} \rangle_s + \delta\hat{a}$ [46]. This approximation assumes the existence of a steady-state $\langle \hat{a} \rangle_s$ of the system, which should be found in the mean-field approximation of the nonlinear dynamical equations of motion. However, in many realistic situations, there does not exist a time-independent or simple harmonic oscillating steady state for the magnomechanical phonon laser. For this reason, we adopt an alternative method for linearizing the system dynamics as in Refs. [22,39–41,47–52].

B. Linearization of dynamics

Referring to Refs. [39–41], we can decompose the total time evolution operator as follows:

$$
\begin{aligned}
\hat{U}(t) &= \hat{T} \exp\left\{ -i \int_0^t ds [\hat{H}_{\mathrm{L}}(s) + \hat{H}_{\mathrm{NL}}(s)] \right\} \\
&= \hat{U}_{\mathrm{L}}(t) \times \hat{T} \exp\left\{ -i \int_0^t ds\, \hat{U}_{\mathrm{L}}^\dagger(s) \hat{H}_{\mathrm{NL}}(s) \hat{U}_{\mathrm{L}}(s) \right\}
\end{aligned}
$$

$$
\begin{aligned}
&= \hat{U}_{\mathrm{L}}(t) \times \hat{T} \exp\left\{ -i \int_0^t ds\, [\hat{H}_1(s) + \hat{H}_2(s)] \right\} \\
&= \hat{U}_{\mathrm{L}}(t) \hat{T} \exp\left\{ -i \int_0^t ds\, \hat{U}_2(t,s) \hat{H}_1(s) \hat{U}_2^\dagger(t,s) \right\} \hat{U}_2(t) \\
&\equiv \hat{U}_{\mathrm{L}}(t) \hat{U}_1(t) \hat{U}_2(t),
\end{aligned} \tag{4}
$$

where $\hat{T}$ indicates the time ordering and $\hat{U}_i(t) = \hat{T} \exp[-i \int_0^t ds\, \hat{H}_i(s)]$. In the second line of this equation, we have decomposed the total time evolution from the left, and in the fourth line we have decomposed the remaining part of the time evolution from the right side. First, we find $\hat{U}_{\mathrm{L}}(t)$ as

$$
\begin{aligned}
\hat{U}_{\mathrm{L}}(t) &= \hat{T} \exp\left[-i \int_0^t \hat{H}_{\mathrm{L}}(s)\, ds \right] \\
&= \exp\Big[-i\omega_a t\, \hat{a}^\dagger \hat{a} - i\omega_m t\, \hat{m}^\dagger \hat{m} - i\omega_b t\, \hat{b}^\dagger \hat{b} \\
&\quad - iJt(\hat{a}^\dagger \hat{m} + \hat{m}^\dagger \hat{a}) + i\frac{E_d}{\omega_d} \hat{m}^\dagger \big(e^{-i\omega_d t} - 1 \big) \\
&\quad + i\frac{E_d}{\omega_d} \hat{m}(e^{i\omega_d t} - 1) \Big].
\end{aligned} \tag{5}
$$

To attain $\hat{U}_{\mathrm{L}}^\dagger(\tau) \hat{H}_{\mathrm{NL}} \hat{U}_{\mathrm{L}}(\tau) \equiv \hat{H}_1(\tau) + \hat{H}_2(\tau)$, we first should obtain $\hat{U}_{\mathrm{L}}^\dagger(\tau) \hat{c} \hat{U}_{\mathrm{L}}(\tau)$, where $\hat{c} = \hat{a}, \hat{m}$, and $\hat{b}$. If $\hat{U}_{\mathrm{L}} \equiv e^{-\hat{G}}$ and $\hat{A}(t) \equiv e^{\hat{G}} \hat{a} e^{-\hat{G}}$, where $\hat{G}^\dagger = -\hat{G}$, then

$$
\frac{d\hat{A}}{dt} = e^{\hat{G}} \left[\frac{d\hat{G}}{dt}, \hat{a} \right] e^{-\hat{G}} = \left[\frac{d\hat{G}}{dt}, \hat{A} \right]. \tag{6}
$$

Similarly, we define $\hat{M}(t) \equiv e^{\hat{G}} \hat{m} e^{-\hat{G}}$ and $\hat{B}(t) \equiv e^{\hat{G}} \hat{b} e^{-\hat{G}}$. After the simplification we obtain

$$
\frac{d}{dt} \begin{pmatrix} \hat{A} \\ \hat{M} \\ \hat{B} \end{pmatrix} = \begin{pmatrix} -i\omega_a & -iJ & 0 \\ -iJ & -i\omega_m & 0 \\ 0 & 0 & -i\omega_b \end{pmatrix} \begin{pmatrix} \hat{A} \\ \hat{M} \\ \hat{B} \end{pmatrix} + \begin{pmatrix} 0 \\ E_d e^{-i\omega_d t} \\ 0 \end{pmatrix}. \tag{7}
$$

We define $\Omega \equiv \frac{1}{2}\sqrt{4J^2 + (\omega_a - \omega_m)^2}$, $\Delta \equiv \omega_a - \omega_m$, and $\eta \equiv \frac{1}{2}(\omega_a + \omega_m)$. Also, noting that $\hat{A}(0) = \hat{a}$, $\hat{M}(0) = \hat{m}$, and $\hat{B}(0) = \hat{b}$, we define the "superoperators" or hybrid photon-magnon modes as

$$
\hat{o}_1 \equiv \frac{\hat{a} + \hat{m}}{\sqrt{2}}, \quad \hat{o}_2 \equiv \frac{\hat{a} - \hat{m}}{\sqrt{2}}. \tag{8}
$$

The superoperators are the orthogonal eigenstates of the Hermitian Hamiltonian $\omega_a \hat{a}^\dagger \hat{a} + \omega_m \hat{m}^\dagger \hat{m} + J(\hat{a}^\dagger \hat{m} + \hat{m}^\dagger \hat{a})$. Then, the solution of Eq. (7) in terms of the supermode operators is

$$
\begin{aligned}
\begin{pmatrix} \hat{A}(t) \\ \hat{M}(t) \\ \hat{B}(t) \end{pmatrix} &= \frac{1}{\sqrt{2}} \begin{pmatrix} \cos(\Omega t) - i\frac{\Delta}{2\Omega}\sin(\Omega t) - i\frac{J}{\Omega}\sin(\Omega t)e^{-i\eta t} & \cos(\Omega t) - i\frac{\Delta}{2\Omega}\sin(\Omega t) + i\frac{J}{\Omega}\sin(\Omega t)e^{-i\eta t} & 0 \\ \cos(\Omega t) + i\frac{\Delta}{2\Omega}\sin(\Omega t) - i\frac{J}{\Omega}\sin(\Omega t)e^{-i\eta t} & -\cos(\Omega t) - i\frac{\Delta}{2\Omega}\sin(\Omega t) - i\frac{J}{\Omega}\sin(\Omega t)e^{-i\eta t} & 0 \\ 0 & 0 & e^{-i\omega_b t} \end{pmatrix} \begin{pmatrix} \hat{o}_1 \\ \hat{o}_2 \\ \hat{b} \end{pmatrix} \\
&\quad + \begin{pmatrix} \frac{iE_d(4\Omega^2 - \Delta^2)}{8J\Omega}\left(\frac{e^{-i(\Omega+\eta)t} - e^{-i\omega_d t}}{\eta + \Omega - \omega_d} + \frac{e^{i(\Omega-\eta)t} - e^{-i\omega_d t}}{\eta + \Omega - \omega_d} \right) \\ \frac{iE_d}{4\Omega}\left(\frac{(2\Omega-\Delta)(e^{-i(\Omega+\eta)t} - e^{-i\omega_d t})}{\eta + \Omega - \omega_d} + \frac{(2\Omega+\Delta)(e^{i(\Omega-\eta)t} - e^{-i\omega_d t})}{\Omega - \eta + \omega_d} \right) \\ 0 \end{pmatrix} \equiv \begin{pmatrix} \alpha_{11} & \alpha_{12} & 0 \\ \alpha_{21} & \alpha_{22} & 0 \\ 0 & 0 & e^{-i\omega_b t} \end{pmatrix} \begin{pmatrix} \hat{o}_1 \\ \hat{o}_2 \\ \hat{b} \end{pmatrix} + \begin{pmatrix} E_1 \\ E_2 \\ 0 \end{pmatrix}.
\end{aligned}
$$

Knowing how A, M, and B evolve with time, we can find $\hat{H}_1$ and $\hat{H}_2$ as

$$\hat{H}_1 = -g(\alpha_{21}E_2^*\hat{o}_1 + \alpha_{22}E_2^*\hat{o}_2 + \alpha_{21}^*E_2\hat{o}_1^\dagger + \alpha_{22}^*E_2\hat{o}_2^\dagger + |E_2|^2)(\hat{B} + \hat{B}^\dagger) \tag{9}$$

and

$$\hat{H}_2 = -g(\alpha_{21}\alpha_{21}^*\hat{o}_1^\dagger\hat{o}_1 + \alpha_{21}\alpha_{22}^*\hat{o}_2^\dagger\hat{o}_1 + \alpha_{22}\alpha_{21}^*\hat{o}_1^\dagger\hat{o}_2 + \alpha_{22}\alpha_{22}^*\hat{o}_2^\dagger\hat{o}_2)(\hat{B} + \hat{B}^\dagger). \tag{10}$$

$\hat{H}_1$ describes the coupling between the two-level system of supermodes and the phonons, and $\hat{H}_2$ is a nonlinear Hamiltonian without being intensified by the pump field (it does not contain a factor of E_d).

We assume the quantum state of our system is the product of a cavity vacuum state and the mechanical thermal state, as well as a vacuum magnon state, i.e., $\rho(0) = |0\rangle_a\langle 0| \otimes |0\rangle_m\langle 0| \bigotimes \sum_{n=0}^\infty n_{\text{th}}/(1 + n_{\text{th}})^{n+1}|n\rangle\langle n|$, where n_{th} is the thermal reservoir mean occupation number, to have $H_2(t)|0\rangle_c = 0$. Having the specific forms of $\hat{H}_1$ and $\hat{H}_2$, we can write the supermode populations as

$$\langle\hat{o}_i^\dagger\hat{o}_i(t)\rangle = \text{Tr}(\hat{U}_2^\dagger(t)\hat{U}_1^\dagger(t)\hat{U}_L^\dagger(t)\hat{o}_i^\dagger\hat{o}_i\hat{U}_L(t)\hat{U}_1(t)\hat{U}_2(t)\rho(0))$$

$$= \text{Tr}(\hat{U}_1^\dagger(t)\hat{U}_L^\dagger(t)\hat{o}_i^\dagger\hat{o}_i\hat{U}_L(t)\hat{U}_1(t)\hat{U}_2(t)\rho(0)\hat{U}_2^\dagger(t))$$

$$= \text{Tr}(\hat{U}_1^\dagger(t)\hat{U}_L^\dagger(t)\hat{o}_i^\dagger\hat{o}_i\hat{U}_L(t)\hat{U}_1(t)\rho(0)), \tag{11}$$

for $i = 1$ and 2, where the action $\hat{U}_2(t)$ does not change the quantum state. The supermode populations $\langle\hat{o}_i^\dagger\hat{o}_i(t)\rangle$, therefore, only evolve as the result of the successive actions of $\hat{U}_L(t)$ and $\hat{U}_1(t)$. In the definition of $\hat{U}_1(t) = \hat{T}\exp[-i\int_0^t ds\hat{U}_2(t,s)\hat{H}_1(s)U_2^\dagger(t,s)]$, we apply the Taylor expansion to $\hat{U}_2$. Since $g \ll \Omega, J, \eta, \omega_a, \omega_m, \gamma_a, \gamma_m$, we can safely neglect all terms including g^2 and higher orders. This is the only approximation we use in the procedure. One should note that the effect of a nonlinear magnomechanical term is included in $\hat{H}_1$ because of the factor g it contains. This approximation, which is independent of the value of E_d, linearizes the equations of motion. Note that the unitary operation $\hat{U}_L(t)$ only displaces the supermode operators in Eq. (11) and the evolution of $\hat{U}_1$ determines the equations of motion.

The action $\hat{U}_1(t)$ of the Hamiltonian $\hat{H}_1$ leads to a system of linear equations [53]:

$$\frac{d}{dt}\hat{o}_1 = -(\alpha_{11}\alpha_{11}^*\gamma_a + \alpha_{21}\alpha_{21}^*\gamma_m)\hat{o}_1 - (\alpha_{12}\alpha_{11}^*\gamma_a + \alpha_{22}\alpha_{21}^*\gamma_m)\hat{o}_2 + ig\alpha_{21}^*E_2(\hat{b}e^{-i\omega_b t} + \hat{b}^\dagger e^{i\omega_b t}) + \lambda_1,$$

$$\frac{d}{dt}\hat{o}_2 = -(\alpha_{11}\alpha_{12}^*\gamma_a + \alpha_{11}\alpha_{22}^*\gamma_m)\hat{o}_1 - (\alpha_{12}\alpha_{12}^*\gamma_a + \alpha_{22}\alpha_{22}^*\gamma_m)\hat{o}_2 + ig\alpha_{22}^*E_2(\hat{b}e^{-i\omega_b t} + \hat{b}^\dagger e^{i\omega_b t}) + \lambda_2,$$

$$\frac{d}{dt}\hat{b} = ig\alpha_{21}E_2^*e^{i\omega_b t}\hat{o}_1 + ig\alpha_{21}^*E_2e^{i\omega_b t}\hat{o}_1^\dagger + ig\alpha_{22}E_2^*e^{i\omega_b t}\hat{o}_2 + ig\alpha_{22}^*E_2e^{i\omega_b t}\hat{o}_2^\dagger - \gamma_b\hat{b} + \lambda_3. \tag{12}$$

Its compact form

$$\frac{d}{dt}\hat{c} = M\hat{c} + \lambda(t), \tag{13}$$

where

$$\hat{c} = (\hat{o}_1, \hat{o}_1^\dagger, \hat{o}_2, \hat{o}_2^\dagger, \hat{b}, \hat{b}^\dagger)^T, \tag{14}$$

and

$$\lambda_1 = -(\gamma_a\alpha_{11}^*E_1 + \gamma_m\alpha_{21}^*E_2),$$
$$\lambda_2 = -(\gamma_a\alpha_{12}^*E_1 + \gamma_m\alpha_{22}^*E_2),$$
$$\lambda_3 = ig|E_2|^2e^{i\omega_b t}, \tag{15}$$

has the solution

$$\hat{c}(t) = \hat{T}\exp\left[\int_0^t d\tau\, M(\tau)\right]\hat{c}(0)$$

$$+ \int_0^t d\tau\, \hat{T}\exp\left[\int_\tau^t ds\, M(s)\right]\lambda(\tau)$$

$$\equiv \hat{c}_s(t) + \hat{c}_{ds}(t), \tag{16}$$

where $\hat{c}_s(t)$ and $\hat{c}_{ds}(t)$ are the homogeneous and inhomogeneous parts of the solution, respectively. We can formally

write

$$\hat{T}\exp\left[\int_\tau^t ds\, M(s)\right]$$

$$= \begin{pmatrix} d_{11}(t,\tau) & d_{12}(t,\tau) & \dots & d_{16}(t,\tau) \\ d_{21}(t,\tau) & d_{22}(t,\tau) & \dots & d_{26}(t,\tau) \\ \vdots & & \ddots & \\ d_{61}(t,\tau) & & & d_{66}(t,\tau) \end{pmatrix}. \tag{17}$$

Since there is no analytical expression for the matrix exponential, we use the following product

$$\hat{T}\exp\left[\int_0^t ds\, M(s)\right] \approx \prod_{i=N-1}^0 (1 + M(s_i)h), \tag{18}$$

where the step size h is chosen so small to assure $M(s_i)M(s_{i+1}) = M(s_{i+1})M(s_i)$, to numerically calculate the evolved operators. We use the algorithm developed in Refs. [22,37] to deal with such evolutions of the system operators.

C. Supermode population inversion

There are two terms in the solution (16). The supermode populations from the first term are obtained by taking the average of $\langle\hat{o}_{i,s}^\dagger\hat{o}_{i,s}(t)\rangle$ with respect to the system's initial state

$\rho(0)$. This part of the contribution is found as

$$\langle \hat{o}_{1,s}^{\dagger} \hat{o}_{1,s} \rangle = d_{21}(t,0)\, d_{12}(t,0) + d_{23}(t,0)\, d_{14}(t,0)$$
$$+ d_{25}(t,0)\, d_{16}(t,0)(n_{\mathrm{th}}+1)$$
$$+ d_{26}(t,0)\, d_{15}(t,0)\, n_{\mathrm{th}} \qquad (19)$$

and

$$\langle \hat{o}_{2,s}^{\dagger} \hat{o}_{2,s} \rangle = d_{41}(t,0)\, d_{32}(t,0) + d_{43}(t,0)\, d_{34}(t,0)$$
$$+ d_{45}(t,0)\, d_{36}(t,0)(n_{\mathrm{th}}+1)$$
$$+ d_{46}(t,0)\, d_{35}(t,0)\, n_{\mathrm{th}}. \qquad (20)$$

Considering the displacement terms due to the action of $\hat{U}_L(t)$, the second pure drive term $\lambda(t)$ yields the following contribution:

$$\langle \hat{o}_{1,ds}^{\dagger} \hat{o}_{1,ds} \rangle = |E_1 + E_2 + \hat{o}_{1,ds}(t)|^2,$$
$$\langle \hat{o}_{2,ds}^{\dagger} \hat{o}_{2,ds} \rangle = |E_1 - E_2 + \hat{o}_{2,ds}(t)|^2, \qquad (21)$$

where

$$\hat{o}_{1,ds} = \int_0^t d\tau \, [d_{11}(t,\tau)\lambda_1 + d_{12}(t,\tau)\lambda_1^* + d_{13}(t,\tau)\lambda_2$$
$$+ d_{14}(t,\tau)\lambda_2^* + d_{15}(t,\tau)\lambda_3 + d_{16}(t,\tau)\lambda_3^*] \qquad (22)$$

and

$$\hat{o}_{2,ds} = \int_0^t d\tau \, [d_{31}(t,\tau)\lambda_1 + d_{32}(t,\tau)\lambda_1^* + d_{33}(t,\tau)\lambda_2$$
$$+ d_{34}(t,\tau)\lambda_2^* + d_{35}(t,\tau)\lambda_3 + d_{36}(t,\tau)\lambda_3^*]. \qquad (23)$$

The quantum noises may modify the result, but their contribution is neglected here because the main source of such contribution due to the thermal environment is proportional to the small damping rate γ_b of the mechanical mode.

After numerically solving Eq. (13) and using Eq. (11), we obtain the total supermode populations as

$$\langle \hat{o}_i^{\dagger} \hat{o}_i \rangle = \langle \hat{o}_{i,s}^{\dagger} \hat{o}_{i,s} \rangle + \langle \hat{o}_{i,ds}^{\dagger} \hat{o}_{i,ds} \rangle. \qquad (24)$$

Then, we define the population inversion as

$$\Delta N = \langle \hat{o}_1^{\dagger} \hat{o}_1 \rangle - \langle \hat{o}_2^{\dagger} \hat{o}_2 \rangle. \qquad (25)$$

This quantity determines the performance of the magnomechanical phonon laser.

III. OPERATION OF THE MAGNOMECHANICAL PHONON LASER

Like an optical laser, the phonon laser demonstrates properties such as threshold, gain saturation, and linewidth narrowing in the lasing regime [19,54–56], but its operation is different. The medium of an optical laser is material, the transition occurs between the energy levels or bands, and the output is an optical beam (cavity mode). On the other hand, the two supermodes of the magnomechanical system form the medium of the phonon laser, the thermal or spontaneous phonons mediate the transition between the supermodes, and the material as a phonon mode provides the output (stimulated phonons) [1,18].

The magnetostriction interaction in magnomechanical systems plays the role of radiation pressure in optomechanical
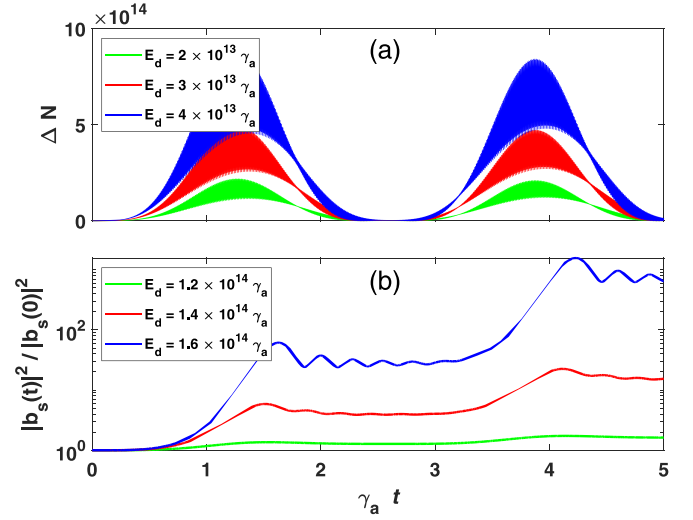

FIG. 2. The population inversion between superoperators for different values of the drive pump. Here we have set $\gamma_a = 2.6$ MHz, $\gamma_m = 1.6$ MHz, $\gamma_b = 628$ Hz, $\omega_a = \omega_m = \omega_d = 20\pi$ GHz (the resonant condition), $\omega_b = 24\pi$ MHz, $J = 2\pi$ MHz, $g = 0.2\pi$ Hz, and $n_{\mathrm{th}} = 2.4 \times 10^5$. (a) One obtains a higher population inversion for a stronger drive pump. The green (bottom), red (middle), and blue (top) curves correspond to drive powers $E_d = 2 \times 10^{13}\, \gamma_a$, $E_d = 3 \times 10^{13}\, \gamma_a$, and $E_d = 4 \times 10^{13}\, \gamma_a$, respectively. (b) The normalized amplified stimulated phonon emission. The green (bottom), red (middle), and blue (top) curves correspond to drive powers $E_d = 1.2 \times 10^{14}\, \gamma_a$, $E_d = 1.4 \times 10^{13}\, \gamma_a$, and $E_d = 1.6 \times 10^{13}\, \gamma_a$, respectively. If we double the drive power, the difference between the amplified stimulated phonon fields is several orders of magnitude in long time scales. We have used stronger drive pump powers in panel (b).

systems. However, unlike the radiation pressure force, the magnetostrictive force is highly tunable via the external magnetic fields. This feature allows one to achieve a controllable phonon laser [24]. Building up a mechanical mode by magnetostriction is the foundation for such phonon lasing. We can describe the whole process as follows. Initially, we place the magnetic sample in the microwave cavity. The uniform magnetic field B generates a uniform magnon (Kittel) mode in the magnetic sphere. On the other hand, the time-dependent magnetic field of the microwave drive excites the magnons harmonically, and the magnetostriction effect deforms the magnetic sphere sinusoidally, converting it to a resonator. Now the system can be modeled by three types of quantized oscillations: the first one stands for the microwave cavity field, which is between two mirrors; the second represents the magnetization in the magnetic sample; and the third is the stimulated mechanical oscillation over the magnetic sphere. The magnetic dipole interaction $\hat{H}_{\mathrm{dip}}$ couples the quantized microwave cavity field (photons) to the quantized magnons, and the magnomechanical interaction $\hat{H}_M$ couples the magnons with the phonons. The magnons and microwave photons of the coupled resonators form the superoperators defined in Eq. (8). This process is similar to the optomechanical system of two coupled whispering-gallery-mode resonators in which the circulating photons in each one form the hybrid modes or supermodes [22]. We define the superoperators as the symmetric and antisymmetric combinations of
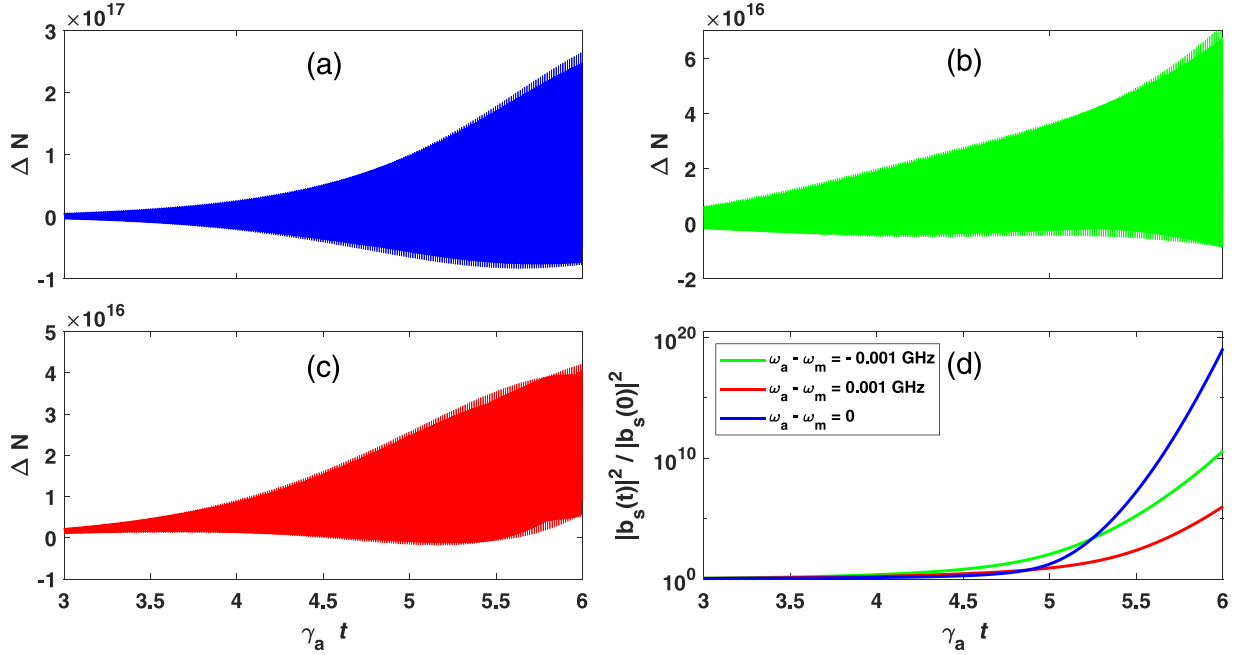
FIG. 3. (a)–(c) The population inversion for the same parameters used in Fig. 2, but here we allow a nonzero detuning between the frequencies of the cavity photons and the magnons. In panel (a), the system is in resonant condition. The panels (b) and (c) correspond to $\omega_a - \omega_m = 0.01$ GHz and $\omega_a - \omega_m = -0.01$ GHz, respectively. The population inversion is 1 order of magnitude larger than these nonresonant cases. (d) The amplified phonon emission for the same parameters used in panels (a)–(c): blue (top) curve for panel (a), green (middle) curve for panel (b), and red (bottom) curve for panel (c). To obtain a strong phonon emission, the detuning must be smaller than 1 MHz.

magnon and photon modes, and they form a two-level system (TLS).

The microwave drive pump excites the mechanical mode associated with the quantized phonons in the magnetic sample. These phonons, which we call "thermal phonons," mediate the transition between the upper and lower levels of the TLS and will be amplified to the stimulated phonon field under the condition of population inversion. One can draw an analogy between the spontaneous and stimulated emission in an optical laser and the thermal and stimulated phonons in a phonon laser. To achieve a reasonably strong stimulated phonon field, one should provide a high population inversion condition between the supermodes. As discussed in the previous section, the population inversion is a dynamical quantity, whereas in, e.g., Refs. [18–20,23], it is treated as a constant value. Similar to an optical laser [44], the phonon laser dynamical equations take the following forms [18,19,22,37],

$$\frac{db_s}{dt} = (-\gamma_b - i\omega_b)b_s - i\frac{g}{2}p,$$

$$\frac{dp}{dt} = i\frac{g}{2}\Delta N(t)b_s + (-\gamma_a - \gamma_m - 2iJ)p, \quad (26)$$

by plugging in the dynamically evolving $\Delta N(t)$, where $p = \langle \hat{o}_2^\dagger \hat{o}_1 \rangle$. In Eq. (26) we have used a subscript "s" to indicate the stimulated phonon field. The variables in Eq. (26) are mean-field ones, but the population inversion $\Delta N(t)$ is determined quantum mechanically. This is similar to the semiclassical treatment of an atomic level transition, in which the atomic levels are described quantum mechanically while the radiations are regarded as classical. Because of the mean-field treatment, there are no noise terms in Eq. (26). After

we numerically solve the system of differential equations in Eq. (26), we obtain the intensified field $b_s(t)$. In the following section, we demonstrate the dynamical evolutions of the population inversion ΔN and the amplification ratio for the phonon number $|b_s(t)/b_s(0)|^2$. Here we use the parameters close to the experimental values used in other setups [31].

IV. PHONON LASING UNDER VARIOUS SYSTEM CONDITIONS

A. Relevance of the pump power

We are interested in knowing how the population inversion and the stimulated phonon emission vary under different conditions. In the first case, we assume all parameters are fixed, except the drive pump E_d. In Fig. 2, we choose these parameters: $\gamma_m = 1.6$ MHz, $\gamma_b = 628$ Hz, $\omega_a = \omega_m = \omega_d = 20\pi$ GHz (the resonant condition), $\omega_b = 24\pi$ MHz, $J = 2\pi$ MHz, $g = 0.2\pi$ Hz, and $n_{th} = 2.4 \times 10^5$. In the numerical calculations, we choose γ_a as the parameter to normalize all other parameters so that the algorithm works with the dimensionless parameters. Here E_d is a variable, with its order of magnitude being 10^{13} in Fig. 2(a) and being 10^{14} in Fig. 2(b).

Figure 2(a) shows that the population inversion demonstrates a pattern of the fast oscillations modulated by a slow oscillation, like in a wave packet with a certain envelope. Similar to the optomechanical phonon laser, where the oscillation of the mechanical mode brings about the sidebands with the multipliers of the mechanical frequency to the cavity fields, the mechanical mode here induces those sidebands to the magnon field and the cavity field, thus leading to the different oscillating components of the supermodes. As we increase the power of the drive pump, we obtain a higher population
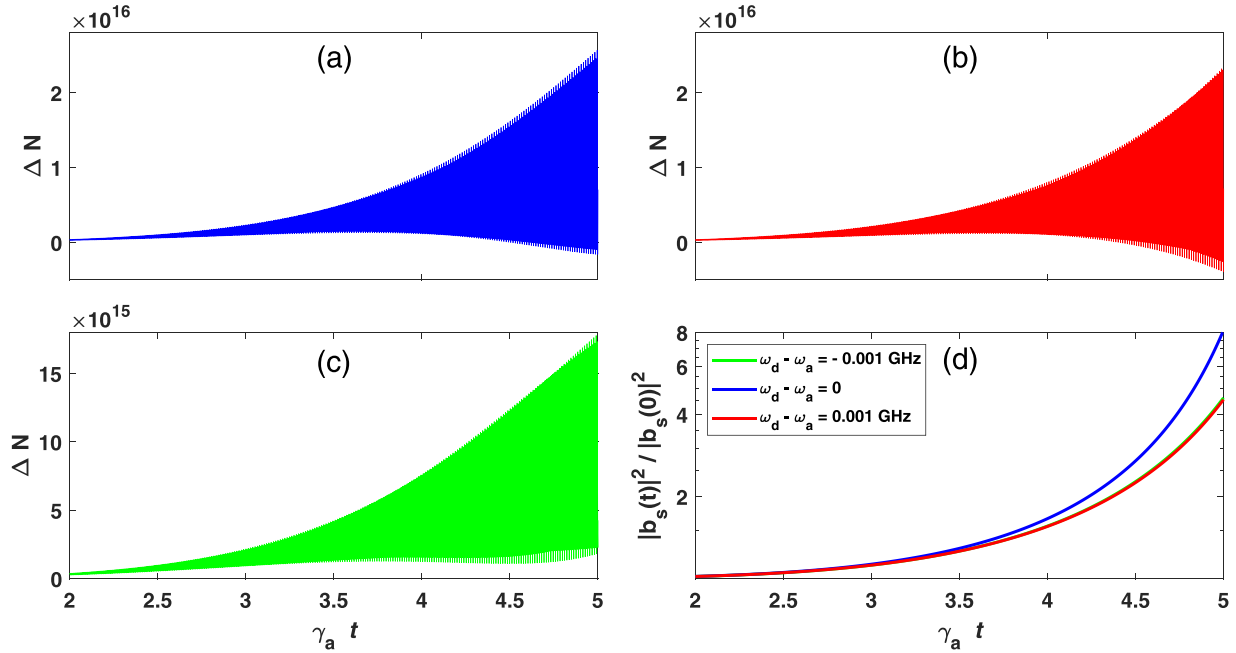
FIG. 4. (a)–(c) The population inversion for the same parameters used in Fig. 3, but here we allow a nonzero detuning between the frequencies of the drive pump and those of the cavity photons and the magnons. Panel (a) shows the system in the resonant condition. Panels (b) and (c) correspond to $\omega_d - \omega_a = 0.001$ and $\omega_d - \omega_a = -0.001$ GHz, respectively. To have a reasonably large population inversion, the detuning should be smaller than 1 MHz. (d) The amplified phonon emission for the same parameters used in panels (a)–(c): blue (top) curve for panel (a) and red (bottom) (curve) for panels (b) and (c). The green curve is coincident on the red curve and, hence, invisible. Here there is no stimulated phonon emission for the negative detuning.

inversion, but the maximum and the minimum in its evolved envelops still occur at where they are for a lower pump power. We also observe the same behavior for the stimulated phonon emission—a stronger phonon emission is achieved for higher drive power in Fig. 2(b). The time-dependent magnetic field in the cavity increases with the power of the drive pump, to have a more intense magnetostriction interaction and, hence, a better phonon lasing.

B. Detuning effect

In addition to the drive pump power and the magnon-photon coupling strength, the resonance condition of the system can affect the phonon laser operation. In Fig. 3, we fix the values of the drive pump power and the magnon-photon coupling strength to $E_d = 5 \times 10^{13} \gamma_a$ and $J = 2\pi \times 10^5 \gamma_a$, but allow a nonzero detuning of $\omega_a - \omega_m = \pm 0.001$ GHz. As we observe in Figs. 3(a)–3(c), the population inversion can be 1 order of magnitude larger in the resonant condition. Also, the amplified phonon emission is much larger under the resonant condition after a long duration for those values of detuning. The detuning is relatively large (10^6 Hz). Thus one can see that, to have the best operation, the detuning must be less than 1 MHz, so as not to affect the population inversion and the phonon emission substantially.

We also investigate the mismatch between the frequency of the drive pump ω_d and that of the cavity photon ω_a and the magnon ω_m. As we expect, the patterns in Figs. 3(a)–3(d) also exist in Figs. 4(a)–4(d), where we use the same parameters as those in Fig. 3, but fix $\omega_a = \omega_m = 20\pi$ GHz and allow a variable ω_d. In Fig. 4(a), the system is in the resonant condition.

In Figs. 4(b) and 4(c), we set $\omega_d - \omega_a = 0.001$ GHz and $\omega_d - \omega_a = -0.001$ GHz, respectively. Particularly, in Fig. 3(d), one sees that no phonon lasing will exist when the detuning is $\omega_d - \omega_a = -0.001$ GHz. An analog in photon laser is that, if one drives a two-level atom at a frequency very different from the transition frequency, no lasing will occur as well. To the currently concerned phonon laser, there will not be an efficient phonon field amplification if the pump frequency mismatches the frequencies of the cavity photon and magnon.

V. DISCUSSION AND CONCLUSION

Similar to an optical laser, one has the gain and the threshold for the magnomechanical laser. The gain of an optical laser depends on the population inversion between the ground state and the excited state. The larger the population inversion is, the higher the gain of the field will be. Furthermore, in an optical laser, the pump power should be beyond a "threshold" to provide the condition of population inversion. The same argument is valid to the concerned phonon laser. In contrast to the steady-state assumption, we here target the more general situation that the population inversion can be time dependent, so we adopt a different approach to the linearization of the system dynamics and an analysis of the population inversion in a numerical way.

It is also possible to study the pulsed phonon laser in the approach we adopt. The pump field $E_d(t)$ can take any form in principle, and a sufficiently strong pump in pulses may give rise to a pulsed output of the stimulated phonon field. This issue should be studied with a further improved numerical tool in the future.

In summary, we have studied a magnomechanical phonon laser beyond the steady-state approximation. Our numerical simulations show that the population inversion between the upper and lower supermodes of the system constantly varies with time, in contrast to an assumption of constant population inversion in the previous studies. We investigate the phonon laser performance, in terms of the population inversion and stimulated phonon field under various system conditions, such as the pump powers, magnon-photon couplings, and detunings. Despite the time-dependent population inversion, one can achieve a relatively strong emission of stimulated phonons if the power of the drive pump is beyond a threshold. The increase of the pump power enables a stronger phonon lasing. A lower magnon-photon coupling can lead to a higher population inversion and a better phonon lasing. Moreover, the phonon laser will have the optimum operation when the frequency of the drive field matches the frequencies of the cavity photons and magnons. Since the magnomechanical system we consider is highly tunable with low loss and has an extra degree of freedom provided by a magnetic field, it can work as an alternative to a phonon laser based on optomechanical systems.

[1] J. Zhang, B. Peng, Ş. K. Özdemir, K. Pichler, D. O. Krimer, G. Zhao, F. Nori, Y.-X. Liu, S. Rötter, and L. Yang, Nat. Photonics **12**, 479 (2018).

[2] J. B. Khurgin, Physics **3**, 16 (2010).

[3] L. Swenson, A. Cruciani, A. Benoit, M. Roesch, C. Yung, A. Bideaud, and A. Monfardini, Appl. Phys. Lett. **96**, 263511 (2010).

[4] H. Shin, J. A. Cox, R. Jarecki, A. Starbuck, Z. Wang, and P. T. Rakich, Nat. Commun. **6**, 6427 (2015).

[5] A. Ganesan, C. Do, and A. Seshia, Phys. Rev. Lett. **118**, 033903 (2017).

[6] M. Serra-Garcia, V. Peri, R. Süsstrunk, O. R. Bilal, T. Larsen, L. G. Villanueva, and S. D. Huber, Nature (London) **555**, 342 (2018).

[7] N. Li, J. Ren, L. Wang, G. Zhang, P. Hänggi, and B. Li, Rev. Mod. Phys. **84**, 1045 (2012).

[8] R. Fleury, D. L. Sounas, C. F. Sieck, M. R. Haberman, and A. Alù, Science **243**, 516 (2014).

[9] D. Hatanaka, I. Mahboob, K. Onomitsu, and H. Yamaguchi, Appl. Phys. Lett. **102**, 213102 (2017).

[10] H. Han, B. Li, S. Volz, and Y. A. Kosevich, Phys. Rev. Lett. **114**, 145501 (2015).

[11] S. R. Sklan, AIP Adv. **5**, 053302 (2015).

[12] K. Vahala, M. Herrmann, S. Knünz, V. Batteiger, G. Saatho, T. Hänsch, and T. Udem, Nat. Phys. **5**, 682 (2009).

[13] J. Kabuss, A. Carmele, T. Brandes, and A. Knorr, Phys. Rev. Lett. **109**, 054301 (2012).

[14] J. Kabuss, A. Carmele, and A. Knorr, Phys. Rev. B **88**, 064305 (2013).

[15] A. Khaetskii, V. N. Golovach, X. Hu, and I. Zutic, Phys. Rev. Lett. **111**, 186601 (2013).

[16] R. P. Beardsley, A. V. Akimov, M. Henini, and A. J. Kent, Phys. Rev. Lett. **104**, 085501 (2010).

[17] I. Mahboob, K. Nishiguchi, A. Fujiwara, and H. Yamaguchi, Phys. Rev. Lett. **110**, 127202 (2013).

[18] I. S. Grudinin, H. Lee, O. Painter, and K. J. Vahala, Phys. Rev. Lett. **104**, 083901 (2010).

[19] H. Jing, Ş. K. Özdemir, X.-Y. Lü, J. Zhang, L. Yang, and F. Nori, Phys. Rev. Lett. **113**, 053604 (2014).

[20] Y. Jiang, S. Maayani, T. Carmon, F. Nori, and H. Jing, Phys. Rev. Applied **10**, 064037 (2018).

[21] R. M. Pettit, W. Ge, P. Kumar, D. R. Luntz-Martin, J. T. Schultz, L. P. Neukirch, M. Bhattacharya, and A. N. Vamivakas, Nat. Photonics **13**, 402 (2019).

[22] B. He, L. Yang, and M. Xiao, Phys. Rev. A **94**, 031802(R) (2016).

[23] M.-S. Ding, L. Zheng, and C. Li, Sci. Rep. **9**, 15723 (2019).

[24] Y. Xu, J.-Y. Liu, W. Liu, and Y.-F. Xiao, Phys. Rev. A **103**, 053501 (2021).

[25] C. Kittel, Introduction to Solid State Physics, 8th ed. (Wiley, New York, 2004).

[26] X. Zhang, C.-L. Zou, L. Jiang, and H. X. Tang, Phys. Rev. Lett. **113**, 156401 (2014).

[27] Y.-P. Wang, G.-Q. Zhang, D. Zhang, X.-Q. Luo, W. Xiong, S.-P. Wang, T.-F. Li, C.-M. Hu, and J. Q. You, Phys. Rev. B **94**, 224410 (2016).

[28] J. A. Haigh, S. Langenfeld, N. J. Lambert, J. J. Baumberg, A. J. Ramsay, A. Nunnenkamp, and A. J. Ferguson, Phys. Rev. A **92**, 063845 (2015).

[29] X. Zhang, N. Zhu, C.-L. Zou, and H. X. Tang, Phys. Rev. Lett. **117**, 123605 (2016).

[30] J. A. Haigh, A. Nunnenkamp, A. J. Ramsay, and A. J. Ferguson, Phys. Rev. Lett. **117**, 133602 (2016).

[31] X. Zhang, C.-L. Zou, L. Jiang, and H. X. Tang, Sci. Adv. **2**, e1501286 (2016) and see supplemental material.

[32] Y. Tabuchi, S. Ishino, A. Noguchi, T. Ishikawa, R. Yamazaki, K. Usami, and Y. Nakamura, Science **349**, 405 (2015).

[33] D. Lachance-Quirion, Y. Tabuchi, S. Ishino, A. Noguchi, T. Ishikawa, R. Yamazaki, and Y. Nakamura, Sci. Adv. **3**, e1603150 (2017).

[34] R. Hisatomi, A. Osada, Y. Tabuchi, T. Ishikawa, A. Noguchi, R. Yamazaki, K. Usami, and Y. Nakamura, Phys. Rev. B **93**, 174427 (2016).

[35] A. V. Chumak, V. I. Vasyuchka, A. A. Serga, and B. Hillebrands, Nat. Phys. **11**, 453 (2015).

[36] D. Lachance-Quirion, Y. Tabuchi, A. Gloppe, K. Usami, and Y. Nakamura, Appl. Phys. Express **12**, 070101 (2019).

[37] Y. F. Xie, Z. Cao, B. He, and Q. Lin, Opt. Express **28**, 22580 (2020).

[38] K. M. Krishnan, Fundamentals and Applications of Magnetic Materials (Oxford University, Oxford, 2016).

[39] B. He, Phys. Rev. A **85**, 063820 (2012).

[40] Q. Lin, B. He, R. Ghobadi, and C. Simon, Phys. Rev. A **90**, 022309 (2014)

[41] Q. Lin, B. He, and M. Xiao, Phys. Rev. Applied **13**, 034030 (2020).

[42] M.-S. Ding, L. Zheng, and C. Li, J. Opt. Soc. Am. B **37**, 627 (2020).

[43] A. Imamoglu, Phys. Rev. Lett. **102**, 083602 (2009).

[44] M. O. Scully and M. S. Zubairy, *Quantum Optics* (Cambridge University, Cambridge, England, 1997).

[45] B. He, L. Yang, Z. Zhang, and M. Xiao, Phys. Rev. A **91**, 033830 (2015).

[46] M. Aspelmeyer, T. J. Kippenberg, and F. Marquardt, Rev. Mod. Phys. **86**, 1391 (2014).

[47] Q. Lin and B. He, Opt. Express **26**, 33830 (2018).

[48] C. Wang, Q. Lin, and B. He, Phys. Rev. A **99**, 023829 (2019).

[49] Q. Lin, B. He, and M. Xiao, Phys. Rev. A **96**, 043812 (2017).

[50] B. He, L. Yang, Q. Lin, and M. Xiao, Phys. Rev. Lett. **118**, 233604 (2017).

[51] Q. Lin and B. He, Opt. Express **23**, 24497 (2015).

[52] B. He, S.-B. Yan, J. Wang, and M. Xiao, Phys. Rev. A **91**, 053832 (2015).

[53] C. Gardiner and P. Zoller, *Quantum Noise* (Springer, Berlin, 2004).

[54] H. Wu, G. Heinrich, and F. Marquardt, New J. Phys. **15**, 123022 (2013).

[55] H. Wang, Z. Wang, J. Zhang, Ş. K. Özdemir, L. Yang, and Y.-X. Liu, Phys. Rev. A **90**, 053814 (2014).

[56] H. Lü, Ş. K. Özdemir, L.-M. Kuang, F. Nori, and H. Jing, Phys. Rev. Applied **8**, 044020 (2017).